Cellulose (2014) 21:4595–4606
DOI 10.1007/s10570-014-0425-x

ORIGINAL PAPER

Structure of swollen carboxylated cellulose fibers

Goeun Sim · Md Nur Alam · Louis Godbout · Theo van de Ven

Received: 22 June 2014 / Accepted: 30 August 2014 / Published online: 12 September 2014

Abstract Structural changes in cellulose fibers were elucidated for carboxymethylated fibers and fibers that are oxidized by periodate and chlorite. Non-fibrillated and partially fibrillated softwood, kraft fibers (SKF, m-SKF) were carboxymethylated to investigate the contribution of the S1 layer to the swollen fiber structures. Carboxymethylated non-fibrillated fibers (CMF) form balloon-like structures as they swell heterogeneously. When partially fibrillated SKF is carboxymethylated (m-CMF), the fibers do not exhibit this ballooning phenomenon due to the degradation of the S1 layer. Carboxymethylation disrupts the native cellulose crystalline structure without breaking the fibers apart. Periodate–chlorite oxidized fibers, on the other hand, swell homogeneously without disrupting the native cellulose I crystalline form. Periodate–chlorite oxidation damages all three secondary layers to the extent that any microfibril confinement caused by the swelling is removed. Each chemistry and mechanical treatment affects the cellulose fibers differently to yield various swollen structures.

Keywords Carboxylated cellulose fiber · Wood fiber swelling · Secondary layers (S1, S2, S3)

G. Sim · M. N. Alam · L. Godbout · T. van de Ven (✉)
Department of Chemistry, Pulp and Paper Research Centre, Centre for Self-Assembled Chemical Structures, McGill University, Montreal, QC, Canada
e-mail: theo.vandeven@mcgill.ca

Introduction

Cellulose wood fibers are highly complex, multilayer composites that serve the role of maintaining the structure of green plants (Ritter 1928; O'Sullivan 1997). The wood cell wall can be divided into the middle lamella (ML), the primary wall (P), and the secondary wall (S) (Déjardin et al. 2010; Tabet and Aziz 2013). Secondary layers (S) of the wood cell wall are mainly composed of helically wound reinforcing cellulose fibrils (Booker and Sell 1998); hence, the S layers are resistant to chemical pulping processes which remove almost all lignin and some hemicelluloses. The ML and P, with high lignin content, on the other hand, are almost completely disintegrated after the pulping process (Whiting and Pulp 1981).

The secondary layer can be further divided into three successive layers, namely, S1, S2, and S3 (Zhong and Ye 2001). The outermost S1 and the innermost S3 layers have 100–200 nm thin walls with microfibril orientation almost perpendicular to the fiber axis (microfibril angles, MFA, 70°–90°). S2 is the thickest layer ($\sim$5 μm) in the cell wall with MFA 7°–40° and it is considered to be one of the dominant determinants of the wood fiber strength (Gustafsson et al. 2003). Structural studies of the wood cell walls have focused mainly on the S2 layer properties and only little is known about the S1 and S3 layers (Gibson 2012).

One of the emerging areas in the cellulose industry is the development of superabsorbent materials. The

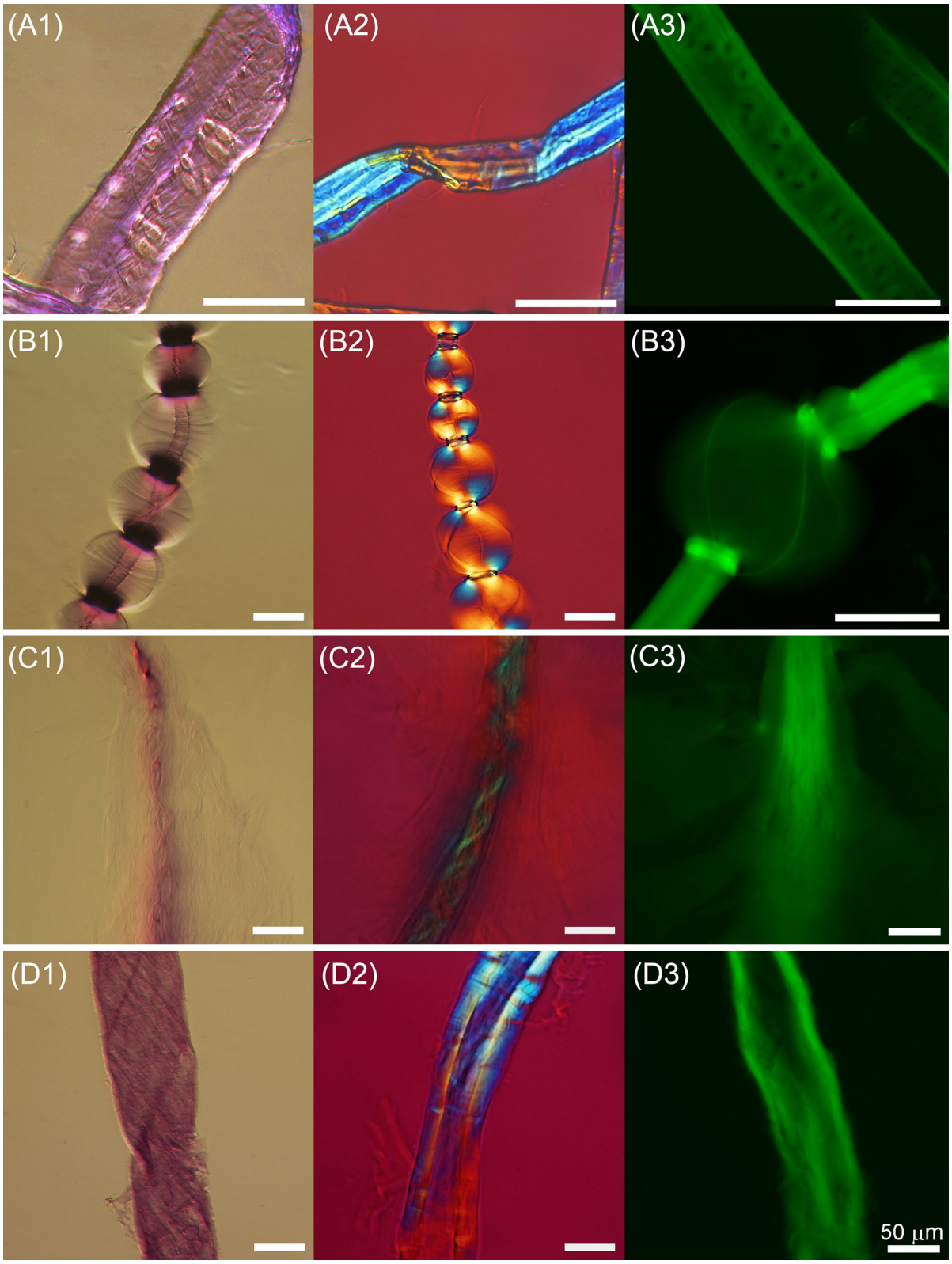
(A1)
(A2)
(A3)
(B1)
(B2)
(B3)
(C1)
(C2)
(C3)
(D1)
(D2)
(D3)
50 μm

◀**Fig. 1** Hoffman modulation contrast light microscopy (HMC) of cellulose fibers dyed with toluidine blue (*A1*, *B1*, *C1*, *D1*); cross-polarized light microscopy, first order retardation plate inserted (*A2*, *B2*, *C2*, *D2*); confocal microscopy, samples dyed with A-fluo. Images are taken with an exposure time of 600 ms and are later z-stacked (*A3*, *B3*, *C3*, *D3*). Unmodified SKF (*A1*, *A2*, *A3*); CMF (*B1*, *B2*, *B3*, [COOH] = 2.6 mmol/g); m-CMF (*C1*, *C2*, *C3*, [COOH] = 2.5 mmol/g); and PCF (*D1*, *D2*, *D3*, [COOH] = 2.7 mmol/g). All *scale bars* are 50 μm

chemical process required to increase the water retention value of cellulose fibers usually involves carboxylation (Hubbe et al. 2008; Aulin et al. 2009; Lin et al. 2012). The swelling of these modified fibers inevitably alters the native fiber structure. Non-uniform swelling of cellulose fibers and how it leads to the formation of balloons was first reported more than a century ago (Nägeli 1864). Since then, an extensive amount of work has been done to understand the swelling and dissolution mechanism of cellulose fibers by chemical modification (Stawitz and Kage 1959) or by varying the solvent systems. Ballooning has been reported during the dissolution of fibers in *N*-methylmorpholine-*N*-oxide (NMMO)–water mixtures (Cuissinat and Navard 2006; Jeihanipour et al. 2010), in NaOH at −8 °C (Le Moigne and Navard 2009), in ionic liquids (Cuissinat et al. 2008), and also during mechanical nanofibrillation (Uetani and Yano 2011). Navard and his coworkers have reported different modes of fiber dissolution that could be tuned by varying the solvent quality, and they have also suggested a fiber swelling mechanism. It is worth investigating whether or not the same mechanism holds for the chemically modified fibers, and how the overall swollen morphology is affected by the three S-layers. To our knowledge, differences in swollen fiber structures with respect to the different types of chemistry applied have not been closely examined.

The three most common ways to introduce carboxylate groups onto the cellulose fibers are: carboxymethylation, periodate–chlorite oxidation and 2,2,6,6-tetramethylpiperidine-1-oxyl (TEMPO) radical mediated oxidation. TEMPO-mediated oxidized fibers cannot exceed 1.7 mmol/g of carboxylate contents (Okita et al. 2010), which is not sufficient to induce severe fiber deformation without any post mechanical treatment (Saito et al. 2007). Therefore, only the first two chemistries will be discussed in this work.

Carboxymethylation non-selectively attacks all three –OH groups that are available on cellulose. The reaction is usually carried out in isopropyl alcohol to minimize hydrolysis of sodium chloroacetate (Heinze and Pfeiffer 1999; Khullar et al. 2005). Above 3 mmol/g of carboxylate content, fibers break apart and large amounts of carboxymethylcellulose (CMC) become soluble in water (Tejado et al. 2012). Commercially available CMC typically has an average DS of 0.7, corresponding to 4.2 mmol/g of carboxylate content. As carboxymethylation requires high concentrations of NaOH, portions of the non-derivatized native cellulose I crystals can be mercerized, and then transformed into the cellulose II crystalline allomorph. As carboxymethylation is often used in the industry to produce CMC, the emphasis of most studies is on the optimization of the CMC yield, without relating it to the swelling behaviour itself (Jardeby et al. 2004, 2005a, b).

Periodate oxidation regioselectively converts vicinal –OH groups at C2 and C3 to yield 2,3-dialdehyde cellulose by opening the glucopyranose ring. The aldehyde groups are then further oxidized to form 2,3-dicarboxylic cellulose by chlorite oxidation (Liimatainen and Visanko 2012). According to Tejado et al., this aqueous chemistry spontaneously breaks the fibers apart into both dissolved dicarboxylated cellulose (DCC) and nanofibrils at ∼3 mmol/g of COO content. Unlike carboxymethylation, periodate–chlorite oxidation does not disrupt the cellulose I crystalline form. This reaction has been used in preparing nanofibrillated cellulose or highly charged cellulose nanocrystals (Tejado et al. 2012; Yang et al. 2012).

The objective of this study is to understand how the fiber structure evolves when different chemical and mechanical treatments are applied to wood fibers and to investigate the role of each secondary layer in fiber swelling. Understanding the swollen fiber structure will become particularly important in the preparation of cellulose-based superabsorbent materials.

Experimental

Materials

Non-fibrillated, bleached softwood kraft fiber sheets (SKF; Domtar, Canada) and partially fibrillated—mechanically treated—SKF (m-SKF, refined 4 times in a disc refiner with refining energy of 33 kWh/t; FPInnovations, Canada) from spruce were used as native cellulose material. Reagent grade sodium

chloroacetate (MCA), sodium meta-periodate ($NaIO_4$), sodium chloride (NaCl), sodium hydroxide (NaOH), sodium chlorite ($NaClO_2$), hydrochloric acid (HCl), hydrogen peroxide (H_2O_2), *N*-(3-dimethylaminopropyl)-*N*′-ethylcarbodiimide hydrochloride (EDC), and 5-aminofuorescein (A-fluo) were purchased from Sigma-Aldrich and were used as received.

Chemical modification

50 g of SKF sheets were torn into small pieces and soaked in distilled water overnight. The wet pulp was disintegrated by a household tilt-head stand mixer (Kitchenaid, Professional 550 plus), filtered to remove excess water, dried at 50 °C. The dried pulp and sodium chloroacetate solution (100 g MCA in 130 mL water) were mixed together and placed in a 60 °C water bath for 4 h for impregnation. Sodium hydroxide solution (62.5 g NaOH in 100 mL water) was then added and the pulp slurry was left overnight at room temperature. The pulp was then washed by 70–100 % ethanol. The final product (carboxymethylated fibers, CMF, prepared from SKF) was dried at 50 °C and stored at room temperature. The same procedure was repeated for m-CMF, using m-SKF.

SKF was oxidized by the periodate–chlorite reaction to make periodate–chlorite oxidized fibers (PCF) following the method reported by Tejado et al. (2012).

Fluorescent tagging of the carboxyl groups of the fibers

Carboxyl groups of the chemically modified cellulose fibers can be fluorescently tagged via a carbodiimide-mediated coupling reaction as reported by Hu and Hayek (2012). Pulps of 0.1 % consistency (Cs) of (1) SKF, (2) CMF, (3) m-CMF and (4) PCF were mixed with A-fluo and EDC·HCl at pH 4–4.5 for 16 h. A molar ratio of (COOH:A-fluo:EDC·HCl = 1:0.5:1) was used in all cases. Samples were dialyzed for 5 days for purification (Spectra/Por, MWCO 12,000).

Acid hydrolysis of CMF and PCF

As part of the structural studies, the chemically modified fibers were subjected to acid treatment to hydrolyze amorphous region to weaken the structure. 0.1 %w/w CMF and PCF suspensions were subjected to a mild acid hydrolysis using 1 N hydrochloric acid at 50 °C for 2 h under magnetic stirring (250 rpm). Purification was done by dialyzing the sample for 3 days (Spectra/Por, MWCO 12,000).

Characterization

Charge determination

The carboxyl contents of CMF, m-CMF and PCF were measured by conductometric titration (Metrohm 836 Titrando). Titration was performed according to Yang et al. (2012).

Optical microscopy

Cellulose fiber dispersions were observed by Hoffman modulation contrast microscopy (HMC, Nikon Eclipse TE2000-U) and by fluorescence microscopy. In the first case, a few drops of 0.01 %w/v toluidine blue solution were added to the sample suspension at least 30 min prior to imaging. For fluorescence, A-fluo treated fibers were excited at $\lambda = 494$ nm with an exposure time of 6–800 ms. Images were later treated with analysis software ImageJ. The fibers were also observed by cross-polarized microscopy (Nikon Eclipse LV100 POL) in which a first order retardation plate (530 nm) was inserted. In confocal microscopy (Zeiss LSM510; 488 nm, Ar laser, 30 mW), each coverslip was sealed with a spacer (0.12 mm in thickness) to minimize the fiber deformation. All confocal imaging was done in water immersion.

Crystallinity determination

X-ray diffraction analysis was performed (Bruker Discover D8; VANTE C 2D detecto; CuKα radiation, $\lambda = 1.54$ Å) and the X-ray diffractograms were acquired with a 2θ (Bragg angle) range of 10°–30° at a scan rate of 0.005° s^{-1}.

Solid state ^{13}C NMR spectra were acquired (Varian, Agilent VNMRS-400) at 100.5 MHz for both functionality and crystalline structure determination. Samples were packed in 7.5 mm zirconia rotors and spun at 5,500 Hz. Spinning side bands were suppressed using the TOSS sequence. Spectra were acquired using a contact time of 2 ms and a recycle delay of 2 s. Typically 6,000 transients were acquired.

Results and discussion

Microscopic observations of the native and swollen fibers

Native and swollen forms of cellulose wood fibers were observed by Hoffman modulation contrast microscopy, cross-polarizing microscopy, and confocal microscopy (Fig. 1). After delignification, the wood fibers (SKF) become highly porous with a composition consisting of ~80 % cellulose and ~20 % hemicellulose (Duchesne et al. 2001). Bordered and non-bordered pit-holes are clearly seen in Fig. 1A1, as well as in Fig. 1A3. MFA or distinctive boundaries between each S-layers could not be identified. Figure 1A2 depicts retardation colors in SKF, which arises from birefringence of anisotropically oriented native cellulose. Fluorescent tagging of the COO groups on the pulp fibers were done by EDC-supported amidization reaction and conductometric titration results show that typically 20 % of the total COO groups are converted into amides under current experimental conditions. See Fig. 1A3 for stacked 2D images of the SKF. The naturally occurring COO groups on the native cellulose fibrils appear to be sufficiently well-distributed within the fiber wall to make the whole fiber fluorescent.

Carboxymethylated fibers (CMF) start to form "balloons" at [COO] ~1.2 mmol/g. The sizes of the balloons increase with an increasing amount of COO groups. CMF ballooning is a well-known phenomenon and terminal stages of the CMF swelling were first illustrated more than 50 years ago (Stawitz and Kage 1959). Jardeby et al. 2004 hypothesized that the ballooning occurs because wood cells have different reactivity due to their large dimensions and high density, thereby creating balloons and "collars". The maximum balloon size observed was ~200 μm in diameter, which occurred at [COO] = 3.2 mmol/g. Above [COO] = 3.2–3.3 mmol/g, the CMF broke apart and CMC was released in solution. As illustrated in Fig. 1B1, the outer S1 and S2 layers swell and are stretched out in transverse directions. Most cellulosic materials after the chemical modification are contained inside the balloons as the yield is near 100 %. Parallel streaks lying across the balloons are most likely stretched out fibrils from the S1 and S2 layers. Cellulosic materials within the balloons become transparent possibly because (1) their sizes are below the wavelength of the light, and/or (2) the differences in refractive indices between the inside and outside of the balloons become minimal due to the dramatic swelling. Axial compression of the CMF was expected as the fiber diameter can expend up to 6.7 times before the fiber breaks up. Le Moigne et al. reported that there is a maximum contraction ratio that wood fibers can withstand [(initial length of the fiber)/(length of the contracted fiber)]. Above 1.7, the fiber disintegrates (Le Moigne et al. 2010). This suggests that the wood fibers can deform more in the transverse directions than the axial, which is probably due to the low MFA in the S2 layer. The S3 layer with MFA between 75° and 90° was also observed. Brandstrom et al. and Bergander et al. measured the MFA of Norway spruce and they have reported that the MFA of the S3 microfibrils is near 90° (Neagu et al. 2006). This indicates that the S3 layer did not suffer from significant changes in MFA—relative to the direction of the fiber—as much as the outer S1 and S2 layers,

Viewing CMF under the cross-polarizing microscope shows that the CMF stays birefringent and the cellulose chains are crossing perpendicularly at the collars (Fig. 1B2). This observation is comparable with that of wood fibers swollen in a NMMO–water mixture, which also showed cellulose chain orientations that resemble bipolar nematic droplets (Cuissinat and Navard 2006). The authors claim that the birefringence is lost during the ballooning and the bright zones are localized only around the "non-swollen sections" or the collars. Considering that the fiber diameters increased by 3–4 times on average, the volume must have increased by at least 10 times. In other words, birefringence in the swollen region is not necessarily lost, but appears to be less pronounced than in the less- or non-swollen regions simply because of their low cellulose density.

Microfibrils that are surrounding the balloons helically can be seen in Fig. 1B3. The formation of helices of the wood fibers swollen in the NMMO–water mixture was examined by Le Moigne et al. 2010 who have claimed that this is due to the rolling up of the primary (P) layer which is caused by stress imbalances due to the chain extension and the changes in chain orientation that had occurred during the ballooning. As kraft pulping almost completely removes the P layer, the helices that are seen in Fig. 1B3 are most likely caused by the spiral extension of the S1 layer. The more pronounced staining of the

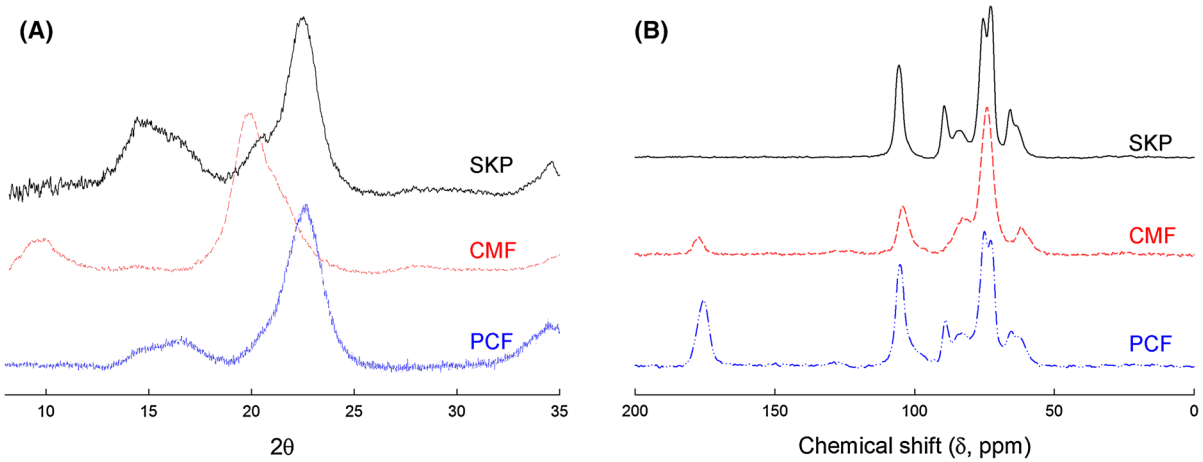

Fig. 2 X-ray diffractograms of air-dried SKF, CMF, and PCF (**a**). Crystalline peak at 22.5° shown in SKF (native crystalline form) remains the same in PCF, but not in CMF. Solid state ^{13}C NMR spectra of SKF, CMF and PCF (**b**). Cellulose I crystalline structure maintained in PCF, but not in CMF. C=O bend at chemical shift 180 ppm from carboxylate content appears in CMF and PCF

collars is due to the fact that the highly charged cellulose chains are more densely packed in the collars than in the balloons. CMF remained highly swollen after fluorescent tagging.

The effect of the S1 layer in fiber swelling was examined by carboxymethylating the partially fibrillated (mechanically treated) SKF (m-SKF). The partial fibrillation was done by refining the high consistency SKF through a disc refiner 4 times, which damages the external fiber surface. The outermost S1 layer and some of the S2 layer are disintegrated by this mechanical treatment. When the m-SKF was subjected to carboxymethylation, the carboxymethylated fibers (m-CMF) swell without forming balloons (Fig. 1C1). The formation of "threads" and "collars" (Le Moigne et al. 2010) must have been prevented by the removal of the S1 layer. This observation agrees with the results reported by Gehmayr et al. (2012), who achieved homogeneous swelling by dissolving the wood fibers after altering the swelling capacity of the P and S1 layers by TEMPO-mediated oxidation. Figure 1C2 shows that birefringent cellulose chains of the S3 layer are also helices with MFA between 40° and 45° when swollen. In the absence of the S1 layer, the surface fibrils of the m-CMF appear to be more dispersed than those of CMF; hence the birefringence appears to be less pronounced in C2. From the diffuse fluorescence in Fig. 1C3, it can be seen that the charges are more uniformly distributed in m-CMF than in CMF.

To understand how different chemistries affect the swollen structure, SKF was modified by a two-step oxidation chemistry: periodate, followed by chlorite oxidation. PCF showed homogeneous swelling without the formation of balloons. PCF begins to swell at [COO] $\sim$1.6 mmol/g and the swollen fiber width increased with an increase of [COO] content. The maximum PCF width observed was $\sim$200 µm, which occurred at [COO] = 3.0 mmol/g. Above [COO] = 3.1 mmol/g, the PCF breaks apart into microfibrils, CNF and DCC (Tejado et al. 2012). As seen in Fig. 1D1, the three S-layers can no longer be distinguished from one another, suggesting that all three S-layers are damaged and swollen homogeneously. Notice that there are multiple microfibrils that are helically surrounding the uniformly swollen PCF, whereas there are only one or two "threads" surrounding the CMF balloons, the remaining ending up in the collars. Little realignment of cellulose microfibrils with respect to the fiber axis seems to have occurred (Fig. 1D2). Glucose ring opening and cellulose chain scission as a side reaction (Whitmore and Bogaard 1994), must have effectively released any constrains that would have caused the formation of collars and balloons by damaging the amorphous regions of the microfibrils. Figure 1D3 again represents the uniformly distributed COO groups inside the fiber wall. Upper part of the fiber appears to be hollow as the thin S3 layer seems to be completely broken up, whereas the lower part of it still shows the remaining S3 layer that has survived the chemical modification.

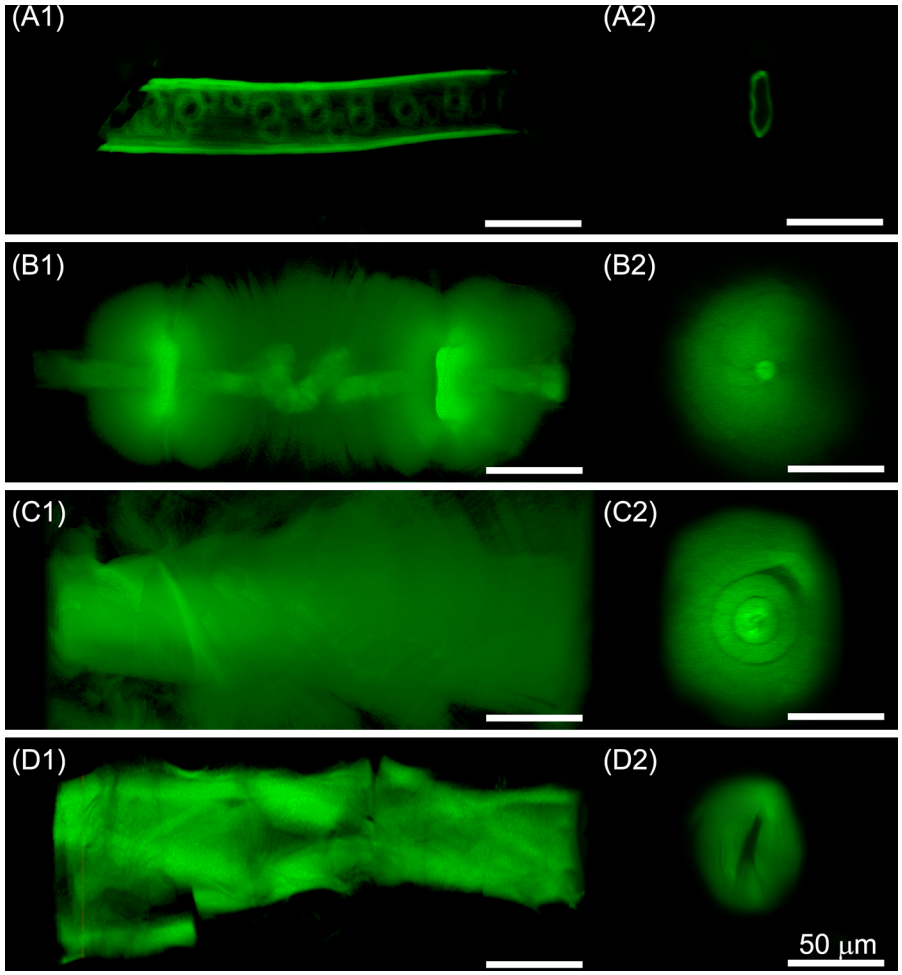

Fig. 3 3D reconstructed images of fibers from confocal microscopy in native form (*A1*, SKF) and swollen forms (*B1*, CMF; *C1*, m-CMF; *D1*, PCF). Cross-sections of each fiber on the right column (*A2*, SKF; *B2*, CMF; *C2*, m-CMF; *D2*, PCF). Images are taken with an exposure time of 800 ms. *Scale bars* are 50 μm

Changes in crystallinity

Carboxymethylation and periodate–chlorite oxidation are similar in a way that –OH groups are carboxylated and that the fibers become more hydrophilic. However, CMF goes through a crystalline structure rearrangement due to the high NaOH concentration used during the carboxymethylation (Yoon et al. 2011). Both X-ray diffraction and ^{13}C solid state NMR spectra (Mittal et al. 2011) confirm that the native crystalline allomorph, cellulose I, is preserved in PCF but not in CMF (See Fig. 2). The cellulose chains that are not carboxymethylated recrystallize in a cellulose II allomorph; hence the CMF rather appears to be a mixture of cellulose II and amorphous cellulose.

Swollen fibers in 3D and their cross-sections

2D confocal microscopic images of wood fibers in native and swollen forms are reconstructed as 3D images (Fig. 3A1, B1, C1, and D1) and their cross-sections are shown in A2, B2, C2, and D2.

SKF is a thin, hollow tube (Fig. 3A1) showing numerous bordered and non-bordered pit holes on its surface. SKF suffers from the lumen collapse which took place at the initial drying process after pulping; hence its cross-section appears to be a wrinkled ellipsoid, not a circle (Fig. 3A2).

Once carboxymethylated, CMF absorbs large amount of water as individual microfibrils swell in all three S-layers (Fig. 3B1). Cellulose chains and

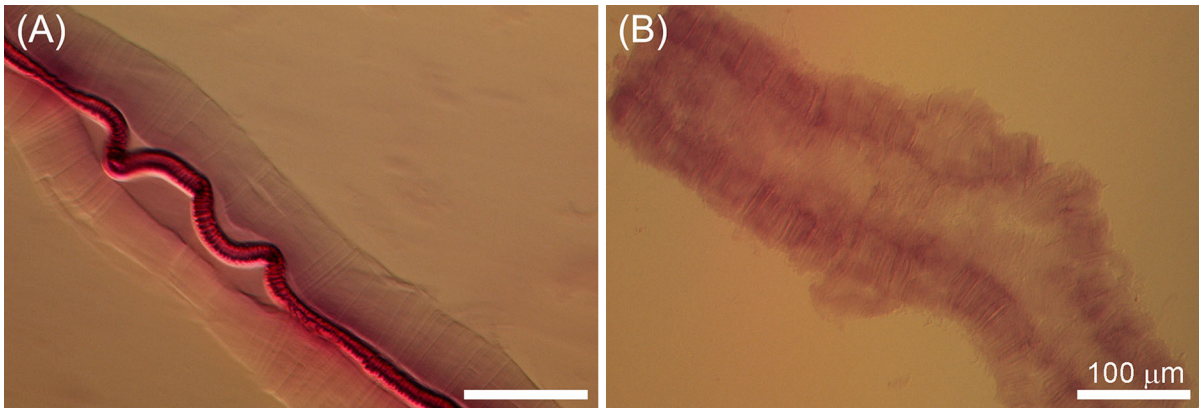

Fig. 4 HMC of acid hydrolyzed CMF (**a**) and PCF (**b**) in 1 N HCl at 50 °C for 2 h. Toluidine blue dyed. *Scale bars* are 100 μm

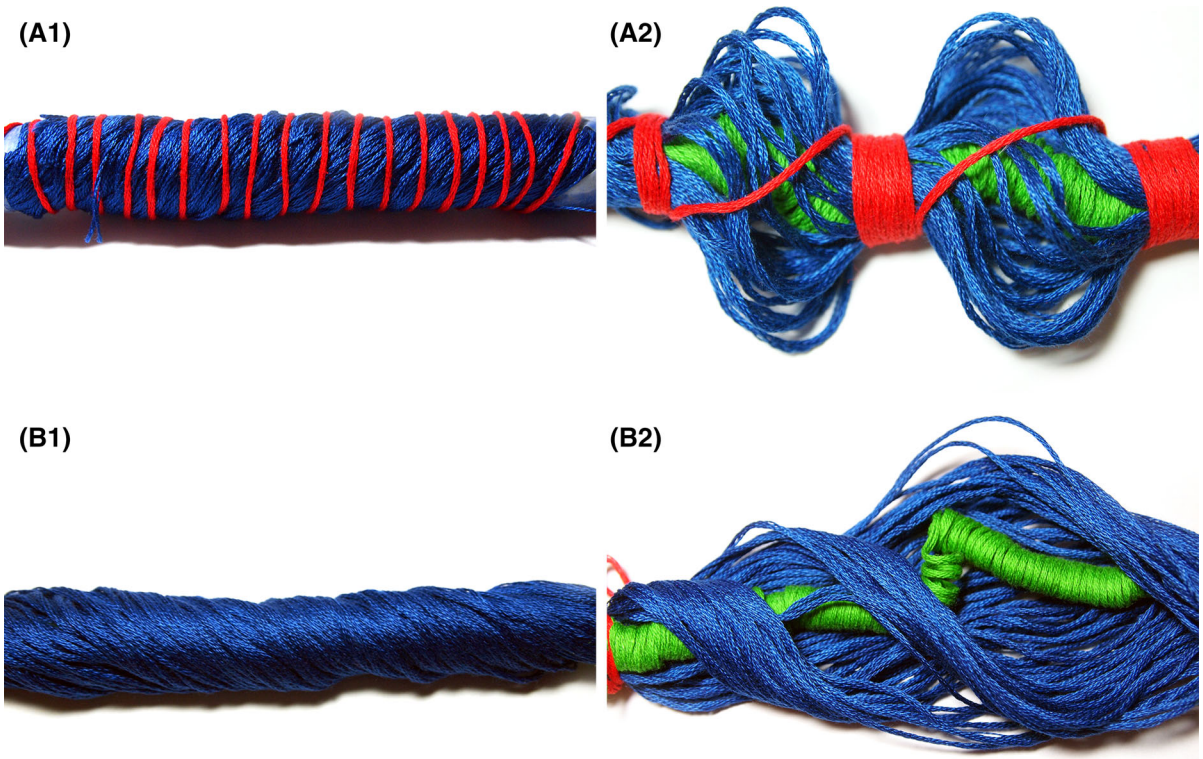

Fig. 5 Fiber swelling was demonstrated using yarns to show how microfibrils behave. Changes mimicking the transition from SKF to CMF are shown in *A1* and *A2*; those from m-SKF to m-CMF are shown in *B1* and *B2*. Fibrils in each layer are represented in *red* (S1), *blue* (S2), and *green* (S3 layer)

hence the attached COO groups too, are densely packed at the collars and the microfibrils in the balloons appear to be oriented almost perpendicular to the fiber axis. This could be explained by the changes in MFA in the S2 layer due to the dramatic stretching in transverse directions. Assuming that the S3 layer can be at least partially separated from the S2 layer, the reduced fiber length due to the transversal stretching can cause the S3 layer to "crumple" inside the balloon. In this paper, we define "crumpling" as the longitudinal deformation of the S3 layer caused by the fiber swelling. It should also be pointed out that the

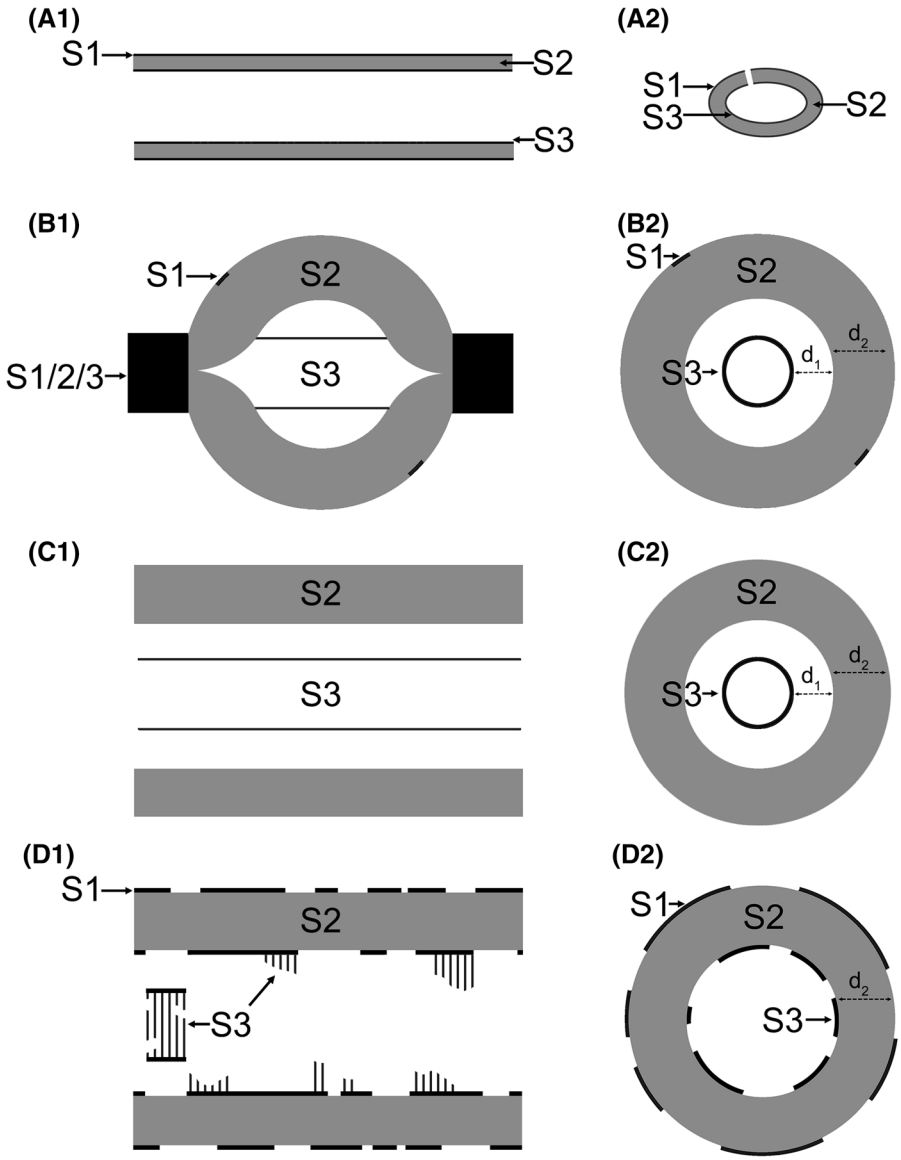

Fig. 6 Schematic representation of **a** SKF; **b** CMF; **c** m-CMF and **d** PCF; longitudinal sections are on the *left column* (*A1–D1*) and cross-sections are on the *right column* (*A2–D2*). The distance between the S2 and S3 layer is denoted as d_1, and thickness of the S2 layer is denoted as d_2. Drawings are approximately to scale

microfibrils in the S3 layer have COO groups on their surface as well, which can be functionalized with A-fluo. From the cross-sectional image of the CMF (Fig. 3B2), it can be seen that the balloons are filled up with highly dispersed cellulose chains and the swollen S3 layer appears to be a circle with 11 μm in diameter.

Mechanically damaging the fiber surface prior to carboxylation prevents ballooning as can be seen in m-CMF. Partially fibrillated and charged surface fibrils are stretched outwards, thereby masking any detailed features inside the swollen fibers when reconstructed in 3D (Fig. 3C1). The cross-section of the m-CMF reveals that the fiber refining has also damaged the outside of the S2 layer (Fig. 3C2). The cross-sectional diameter of m-CMF is about the same as that of CMF.

Periodate–chlorite oxidation results in homogeneous swelling but causes cellulose chain scission. Therefore, the PCF appears to be a hollow tube with imperfections on the fiber surface (Fig. 3D1). The S3 layer must be broken in pieces since it is not visible from the 3D structure, nor from the cross-section (Fig. 3D2). The fiber wall, mostly S2 layer (~5 μm), is typically swollen 5–10 times in total.

One could argue that it is also possible for each secondary layer to have different chemical reactivity; hence the charge contents may vary accordingly. As fibers under tension exhibit reduced reactivity (Le Moigne et al. 2010), the stress generated from the ballooning which has mainly originated from the S2 layer deformation may have suppressed the S3 layer to go through the same degree of chemical conversion as the S2 layer. Nevertheless, the S3 layer still swells as much as 10 times (Fig. 3B2, C2), which is about the same degree of the S2 layer swelling. While the charged S2 microfibrils are stretched out transversely to form balloons, the inner S3 layer is longitudinally compressed and crumpled. This changes cellulose distribution within the fiber, and hence the local charge density, which is directly proportional to the fluorescent intensity. The S3 layer contains charge groups and its microfibrils are densely packed together with high MFA to give a fluorescent intensity comparable to that of the S2 layer.

S2 and S3 layer separation

Acid hydrolysis results in cellulose chain scission as it breaks the glycosidic bond. The CMF and PCF were subjected to a very mild acid hydrolysis to observe how these swollen structures evolve further. After CMF was hydrolyzed for 2 h, the collars and microfibril helices that surrounded the CMF were completely removed (Fig. 4A). A void space between the S2 and S3 layers became visible in the region where S3 is crumpled, which suggests that the fiber swelling, accompanied by a reduction in fiber length, induces the crumpling of the S3 layer and the S2–S3 separation. Compared to CMF, PCF is more prone to fiber disintegration as more cellulose chains are damaged at the same degree of carboxylation. Figure 4B shows that the hydrolyzed PCF surface is not as well-defined as that of hydrolyzed CMF. The inside of the PCF remains hollow as the S3 layer must have been damaged before crumpling occurs. Hydrolyzing PCF readily disintegrates the whole fiber structure, instead of leading to the S2–S3 separation.

Model of fiber swelling

Figure 5 shows a model made with yarns oriented at angles similar to those in a typical fiber. Fibrils in the S1, S2, and S3 layers are color-coded as red, blue, and green. The swelling of SKF and m-SKF was mimicked by simultaneously pulling out the yarns at two different points in directions perpendicular to the fiber axis. Since the S2 layer contains approximately 50 times more microfibrils than the S1 and S3 layers, the driving force in morphological changes must arise from the S2 layer. Therefore, the blue yarns that represent the fibrils in the S2 layer were pulled out and a dramatic increase in their MFA was observed immediately (Fig. 5A2). The red S1 layer experienced both contraction and expansion at the same time, which respectively created collars and spiral coils that go around the balloons. Crumpling of the green S3 layer due to the S2–S3 separation as well as the reduced fiber length was also observed.

To illustrate the effect of the S1 layer on swelling, the red yarn (S1) was removed and the blue yarns (S2) were pulled out in the same manner as before (Fig. 5B2). No ballooning was observed in this case and there was a lesser increase in the MFA of the S2 layer. The S3 layer crumpled inside the highly swollen S2 microfibrils. This indicates that the S1 layer plays a significant role in the formation of balloons, mainly due to their high MFA which constrains the homogeneous swelling of the inner layers.

Schematics of swollen fiber structures

Schematic diagrams of the native and swollen fiber sections are presented in Fig. 6. As seen in Fig. 6A1, the longitudinal section of the unmodified SKF resembles that of the hollow cylinder. Thickness of the S1 and S3 layers are typically 0.1 μm, whereas that of S2 is 5 μm. To make the diagram fit to scale, the S1 and S3 layers are represented as black lines, whereas the S2 layer is shown as a grey shade. Figure 6A2 illustrates the ellipsoidal SKF cross-section with well-defined S1, 2, 3 layers. Chemicals are accessible through the pores and the pit holes, which are represented as a cut.

Once carboxymethylated, all three S-layers swell up to 5–10 times. In Fig. 6B1, collars are represented as black rectangles and this is the area where microfibrils from all three S-layers are located: contracted S1, collared S2, and swollen S3 sitting inside the CMF. The helix created by the spiral extension of the S1 layer is represented as short lines which are diagonally aligned with each other. The highly swollen S2 layer is shown as a grey shade,

where the S3 layer is represented as parallel lines in the longitudinal section (B1) and as a circle in the cross-section (B2). When the fiber crumpling induces the separation between the S2 and S3 layers, the S3 can be positioned anywhere in the empty space. In Fig. 6B2, the distance between the S2 and S3 layer is denoted as d_1, and the thickness of the S2 layer as d_2. The amount of [COO] groups and the crumpling of the S3 layer dictate the magnitude of d_1 and d_2, respectively. In case of no S2–S3 separation or no S3 crumpling, d_1 can be as low as 0, which is the case in Fig. 3B2.

The S1 layer is damaged when passing through a refiner, and therefore it is not shown in either of the m-CMF sections. In Fig. 6C1, the longitudinal section of the homogeneously swollen m-CMF is illustrated. The overall geometry is comparable with that of SKF (Fig. 6A1), except that the S2 and S3 layers are thicker and that the S1 layer is absent in C1. Since the separation of the S3 from the S2 layer is also likely to happen, the cross-sectional image of the m-CMF (Fig. 6C2) resembles that of CMF (Fig. 6B2). The distance range of d_1 and d_2 remains unchanged.

Partially damaged S1 and S3 layers are represented as non-continuous lines in Fig. 6D1 to describe microfibril disintegration that had occurred during periodate–chlorite oxidation. The S2 layer swells to about the same degree as that in CMF; hence d_2 stays the same (Fig. 6D2). On the other hand, the partially broken S1 and S3 layers are still attached to the highly swollen S2 layers; hence $d_1 = 0$ in this case.

Concluding remarks

We have shown that the structure of the swollen wood fibers can be tailored by varying the mechanical and chemical fiber treatments. Carboxymethylated cellulose fibers swell by forming balloon-like structures. Exposure of the fibers to strong alkali during carboxymethylation transforms the native cellulose to cellulose II. Periodate–chlorite oxidation, on the other hand, induces homogeneous swelling while keeping the cellulose crystals in their native form. Damaging the S1 layer by mechanical or chemical means gives rise to homogeneous swelling, which proves that the S1 layer is responsible for the ballooning effect. The thickest secondary layer, S2, experiences a large increase in MFA which reduces the total fiber length. The transversal expansion, accompanied by longitudinal shrinkage of the fibers, causes the crumpling of the S3 layer, thereby leaving an empty space between the S2 and S3 layers.

The key factor in resolving the issue of low accessibility, hence the low reactivity of the cellulose fibers, is the reduction of stress buildup caused by the structural deformation of the fibers. In order to achieve a complete dissolution or a high yield derivatization instead of a heterogeneous mixture of fiber fragments and cellulose nanocrystals (CNC), it is necessary to weaken the structural integrity of the fibers prior to applying any chemical treatments.

Acknowledgments This work was supported by an NSERC Industrial Research Chair supported by FPInnovations, by the NSERC Green Fibre Network, and the FQRNT Centre for Self-Assembled Chemical Structures. Special thanks to Dr. Fred Morin at McGill NMR facility, Dr. Elke Küster-Schöck at McGill Cell Imaging and Analysis Network and Dr. Alois Vanerek for valuable suggestions.

References

Aulin C, Ahola S, Josefsson P et al (2009) Nanoscale cellulose films with different crystallinities and mesostructures—their surface properties and interaction with water. Langmuir 25:7675–7685. doi:10.1021/la900323n

Booker R, Sell J (1998) The nanostructure of the cell wall of softwoods and its functions in a living tree. Holz als Roh- und Werkst 56:1–8. doi:10.1007/s001070050255

Neagu RC, Gamstedt EK, Bardage SL, Lindström M (2006) Ultrastructural features affecting mechanical properties of wood fibres. Wood Mater Sci Eng 1:146–170. doi:10.1080/17480270701195374

Cuissinat C, Navard P (2006) Swelling and dissolution of cellulose part 1: free floating cotton and wood fibres in N-methylmorpholine-N-oxide–water mixtures. Macromol Symp 244:1–18. doi:10.1002/masy.200651201

Cuissinat C, Navard P, Heinze T (2008) Swelling and dissolution of cellulose. Part IV: free floating cotton and wood fibres in ionic liquids. Carbohydr Polym 72:590–596. doi:10.1016/j.carbpol.2007.09.029

Déjardin A, Laurans F, Arnaud D et al (2010) Wood formation in angiosperms. C R Biol 333:325–334. doi:10.1016/j.crvi.2010.01.010

Duchesne I, Hult E, Molin U et al (2001) The influence of hemicellulose on fibril aggregation of kraft pulp fibres as revealed by FE-SEM and CP/MAS 13C-NMR. Cellulose 8:103–111

Gehmayr V, Potthast A, Sixta H (2012) Reactivity of dissolving pulps modified by TEMPO-mediated oxidation. Cellulose 19:1125–1134. doi:10.1007/s10570-012-9729-x

Gibson LJ (2012) The hierarchical structure and mechanics of plant materials. J R Soc Interface 9:2749–2766. doi:10.1098/rsif.2012.0341

Gustafsson J, Ciovica L, Peltonen J (2003) The ultrastructure of spruce kraft pulps studied by atomic force microscopy (AFM) and X-ray photoelectron spectroscopy (XPS). Polymer 44:661–670. doi:10.1016/S0032-3861(02)00807-8

Heinze T, Pfeiffer K (1999) Studies on the synthesis and characterization of carboxymethylcellulose. Die Angew Makromol 266:37–45

Hu TQ, Hayak A (2012) Cellulose materials with novel properties. US Patent. US20120041183 A1

Hubbe M, Rojas O, Lucia L, Sain M (2008) Cellulosic nanocomposites: a review. BioResources 3:929–980

Jardeby K, Lennholm H, Germgård U (2004) Characterisation of the undissolved residuals ID CMC-solutions. Cellulose 11:195–202

Jardeby K, Germgård U, Kreutz B et al (2005a) The influence of fibre wall thickness on the undissolved residuals in CMC solutions. Cellulose 12:167–175. doi:10.1007/s10570-004-1371-9

Jardeby K, Germgård U, Kreutz B et al (2005b) Effect of pulp composition on the characteristics of residuals in CMC made from such pulps. Cellulose 12:385–393. doi:10.1007/s10570-005-2202-3

Jeihanipour A, Karimi K, Taherzadeh MJ (2010) Enhancement of ethanol and biogas production from high-crystalline cellulose by different modes of NMO pretreatment. Biotechnol Bioeng 105:469–476. doi:10.1002/bit.22558

Khullar R, Varshney VK, Naithani S et al (2005) Carboxymethylation of cellulosic material (average degree of polymerization 2600) isolated from cotton (Gossypium) linters with respect to degree of substitution and rheological behavior. J Appl Polym Sci 96:1477–1482. doi:10.1002/app.21645

Le Moigne N, Navard P (2009) Dissolution mechanisms of wood cellulose fibres in NaOH–water. Cellulose 17:31–45. doi:10.1007/s10570-009-9370-5

Le Moigne N, Bikard J, Navard P (2010) Rotation and contraction of native and regenerated cellulose fibers upon swelling and dissolution: the role of morphological and stress unbalances. Cellulose 17:507–519. doi:10.1007/s10570-009-9395-9

Liimatainen H, Visanko M (2012) Enhancement of the nanofibrillation of wood cellulose through sequential periodate–chlorite oxidation. Biomacromolecules 13:1592–1597

Lin N, Bruzzese C, Dufresne A (2012) TEMPO-oxidized nanocellulose participating as crosslinking aid for alginate-based sponges. ACS Appl Mater Interfaces 4:4948–4959. doi:10.1021/am301325r

Mittal A, Katahira R, Himmel ME, Johnson DK (2011) Effects of alkaline or liquid-ammonia treatment on crystalline cellulose: changes in crystalline structure and effects on enzymatic digestibility. Biotechnol Biofuels 4:41. doi:10.1186/1754-6834-4-41

Nägeli C (1864) Über den inneren Bau der vegetabilischen Zellmembranen. Sitzber Bay Akad Wiss Munchen 1: 282–323

O'Sullivan A (1997) Cellulose: the structure slowly unravels. Cellulose 4:173–207. doi:10.1023/A:1018431705579

Okita Y, Saito T, Isogai A (2010) Entire surface oxidation of various cellulose microfibrils by TEMPO-mediated oxidation. Biomacromolecules 11:1696–1700. doi:10.1021/bm100214b

Ritter G (1928) Composition and structure of the cell wall of wood. Ind Eng Chem 20:941–945. doi:10.1021/ie50225a020

Saito T, Kimura S, Nishiyama Y, Isogai A (2007) Cellulose nanofibers prepared by TEMPO-mediated oxidation of native cellulose. Biomacromolecules 8:2485–2491. doi:10.1021/bm0703970

Stawitz VJ, Kage MP (1959) Über die quellungsstadien der wasserlöslichen celluloseäther und die übermolekulare Struktur der Cellulose. Das Papier. 13:567–572

Tabet T, Aziz F (2013) Cellulose microfibril angle in wood and its dynamic mechanical significance. In: van de Ven T, Godbout L (eds) Cellulose—Fundamental Aspects, In-Tech, Croatia, pp 230–257

Tejado A, Alam MN, Antal M et al (2012) Energy requirements for the disintegration of cellulose fibers into cellulose nanofibers. Cellulose 19:831–842. doi:10.1007/s10570-012-9694-4

Uetani K, Yano H (2011) Nanofibrillation of wood pulp using a high-speed blender. Biomacromolecules 12:348–353. doi:10.1021/bm101103p

Whiting P, Pulp DAIG (1981) The topochemistry of delignification shown by pulping middle lamella and secondary wall tissue from black spruce wood. J Wood Chem Technol 1:111–122. doi:10.1080/02773818108085108

Whitmore PM, Bogaard J (1994) Determination of the cellulose scission route in the hydrolytic and oxidative degradation of paper. Restaurator 15:26–45. doi:10.1515/rest.1994.15.1.26

Yang H, Tejado A, Alam N et al (2012) Films prepared from electrosterically stabilized nanocrystalline cellulose. Langmuir 28:7834–7842. doi:10.1021/la2049663

Yoon MJ, Doh SJ, Im JN (2011) Preparation and characterization of carboxymethyl cellulose nonwovens by a wet-laid process. Fibers Polym 12:247–251. doi:10.1007/s12221-011-0247-5

Zhong R, Ye Z-H (2001) Secondary cell walls. Encycl Life Sci 1–9. doi:10.1002/9780470015902.a0021256